Cells Theory of biological force sensing

D5

B. Sabass

Theoretical Soft Matter and Biophysics

Institute of Complex Systems -2

Forschungszentrum Jülich GmbH

Contents

a)

F

10   5   0
force F [N]

analog force measurement
with a reference scale

b)

On

F [0.1 N]

Off

binary force sensor
with a threshold

c)

F [nN]

molecular force sensing in the
cytoskeleton of adherent cells

d)

F [10 pN]

force sensing by cellular
membrane channels

Fig. 1: *Force measurement in our macroscopic world and in molecular systems of biological cells. a) Macroscopic device for analog force measurement consisting of a spring and a ruler. b) A light switch is a binary force sensor that flips if sufficiently strong forces are applied for a sufficiently long time. c) Adherent cells sense and control tensional forces ranging from about 10^{-12} N to about 10^{-9} N. d) Cellular membrane channels detect minute forces resulting from poking, shear flow, or osmotic pressure on the membrane.*

1   Introduction

Mechanotransduction – the cellular transduction of mechanical information into chemical signals – occurs on the level of specialized molecules. During the last decades, a large number of mechanotransduction molecules have been discovered, leading to the general perception that molecular mechanosensors exist in almost all types of cellular organisms, from bacteria to mammalian cells and plant cells. These molecular sensors can not only detect forces but also sense mechanical properties of the environment, including viscosity, pressure, and elastic deformability. For instance, most cells have means to detect tension in their outer membrane, which enables them to maintain their mechanical integrity. Since the molecular underpinnings of biological force sensing are slowly unraveling, there is an obvious need for theory to understand generic mechanisms. This chapter will introduce paradigmatic molecular mechanosensors along with established concepts for theoretical modeling. A few original contributions regarding sensitivity and optimal detection of force changes are also presented.

Measuring minute quantities with molecular sensors may require systems that are quite different from those employed for measurement in our macroscopic world. For instance, we usually measure macroscopic mechanical forces by recording the extension of a spring as shown in Fig. 1. This type of analog measurement is predicated on the availability of a gauged reference scale. Alternatively, one may be more interested in knowing if the force exceeds a given threshold. An example is a bistable light switch. In the nanoscopic world of biological molecules, the

energy scales of the sensor and the signal are not far above the thermal energy scale $k_B T$. Thus, any system is subject to considerable fluctuations, which makes the two exemplary macroscopic measurement approaches hard to realize. Noise affects the gauged reference scale of an analog device as well as the definite state of a binary sensor. The question is then, which strategies are employed by nature to sense and interpret stochastic signals robustly and quickly.

2 Mechanosensitive membrane channels

Mechanosensitive channels are a class of membrane channels that open or close upon mechanical stimulation. When open, they allow passage of ions or solvent through the membrane, thus transducing the mechanical stimulus into a chemical signal. Membrane channels for mechanotransduction are expressed in almost all cells, including prokaryotes and mammalian cells. In fact, our perception of the world ultimately relies on these channels since they are responsible for our sense of touch or pain and enable hearing. Mechanosensitive channels are also required for maintaining tissue integrity, for blood pressure regulation, and osmoregulation [25]. Although the first studies of mechanosensitive channels are more than 30 years old [14], the various biophysical mechanisms of mechanotransduction by membrane channels have only become a very active research field during the last decade [9, 29, 3].

2.1 Tension-sensing membrane channels

One of the best-studied mechanism for cellular mechanotransduction is "tension sensing". The salient feature of the tension sensing mechanism is that membrane channels react to increased tension with shape changes and an ensuing pore opening, see Fig. 2a). Tension-sensing channels were largely studied with bacterial model organisms. Bacteria can grow in environments with various concentrations of salts and sugars, leading to considerable variations in osmotic pressure. It is thought that bacteria have evolved membrane channels that open if the tension in the membrane exceeds a critical level, thereby avoiding deformation and bursting of their outer membrane under osmotic pressure. Channels that could fulfill this function are the mechanosensitive channel with small conductance (MscS) and large conductance (MscL), which open at a tension around $10 \, \mathrm{mN/m}$, approaching the lytic tension of bacterial membranes. A popular physical mechanisms of tension-sensing relies on a radial expansion of the channel molecule [29, 23]. If a channel opens, it changes the area that it occupies in the membrane. Given a finite tension γ of the membrane, the free energy change associated with a positive area change ΔA is $\Delta \mathcal{F} = -\gamma \Delta A$. Denote the state of the channel by x with $x = 0$ being the closed state and $x = 1$ being the open state. Assigning internal energies of ϵ_0 and ϵ_1 to the closed and open states, the overall energy is given by $\mathcal{F}_x(\gamma) = (1 - x)\epsilon_0 + x\epsilon_1 - x\gamma\Delta A$. Assuming equilibrium, the probability of having an open channel is

$$p_1(\gamma) = \frac{e^{-\frac{\mathcal{F}_1(\gamma)}{k_B T}}}{\sum_{x=0,1} e^{-\frac{\mathcal{F}_x(\gamma)}{k_B T}}} = \frac{1}{e^{\frac{\epsilon_1 - \epsilon_0 - \gamma\Delta A}{k_B T}} + 1}. \tag{1}$$

The resulting sigmoidal dependence of the open probability on membrane tension has been measured for various channels. The corresponding data for MscL is shown in Fig. 2c). Such measurements allow to estimate the energy difference between open and closed channel. Having a radius on the order of $R_0 = 2 \, \mathrm{nm}$ in the closed state, the channel area can change up to
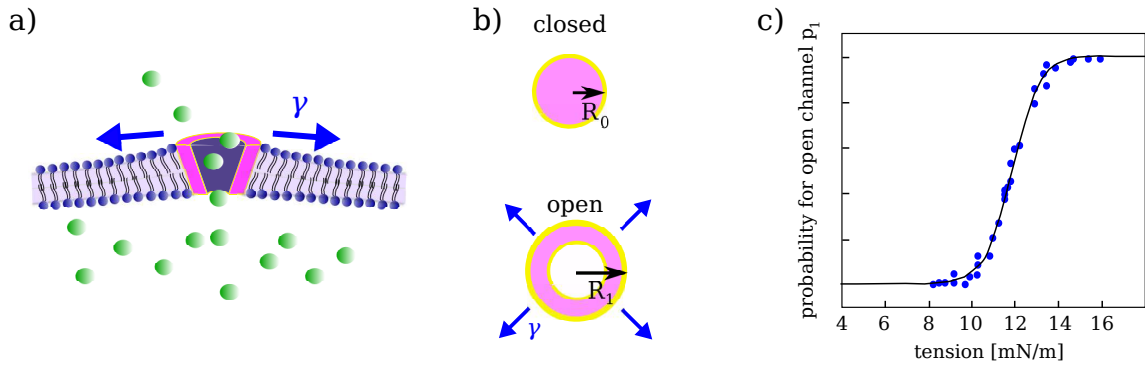
Fig. 2: *a) Sketch of a tension-sensing membrane channel. b) Opening changes the area that the channel occupies. c) Measured opening of MscL and fit to Eq. (1). Data points taken from Ref. [30].*

$\Delta A = \pi(R_1 - R_0) \sim 20\,\mathrm{nm}^2$. Using a typical opening membrane tension of $\gamma = 10\,\mathrm{mN/m}$ we find $\epsilon_1 - \epsilon_0 \sim \gamma \Delta A = 2 \times 10^{-19}\,\mathrm{Nm} \simeq 48\,\mathrm{k_B T}$. This high energetic barrier prevents thermal fluctuations from strongly affecting the opening state. Hence, tension-sensing channels with large area change are molecular sensors that selectively respond to large stimuli that would be critical for the integrity of the cell.

2.2   Channels sensing force through attached tethers

A second mechanism for mechanosensing is based on the idea that forces can be transmitted directly to the channels via attached tethers (Fig. 3a). Tethered channels occur in various biological systems, for instance in nociceptors (harm-sensing neurons) [12] and osmosensory neurons [24]. Notably, it has also been hypothesized that tethered channels are necessary for hearing [15]. On the molecular level, one of the best-studied mechanosensitive ion channels is TRPN, a member of the Transient Receptor Potential channel family. It is responsible for touch sensation and hearing in Drosophila [10, 35]. TRPN has a remarkably long N-terminal module with 29 ankyrin repeats that tethers the channel to intracellular structures. Applying force to the ankyrin tether opens the channel. Interestingly, it has been shown that the ankyrin tether from TRPN can be fused to a voltage-gated potassium channel that is usually mechanoinsensitive, and then renders this channel mechanosensitive [35]. This finding raises the question whether sensing force at tethers could rely on simple micromechanical principles that are somewhat independent of the detailed molecular channel structure.

The physical mechanisms involved in opening of tethered channels are a subject of current research. Certainly, opening in response to force could be based on a rearrangement of the molecule only, which may be thought of as "trap door mechanism", see Fig. 3b). However, it is likely that the energetics of the membrane-channel interaction also play a role for opening [27]. In particular, conical deformations of the channel shape affect the membrane bending energy. To estimate the energetic effect of conical deformations, we consider the system depicted in Fig. 3a), where a channel connected to a tether bears a force F on the order of $10\,\mathrm{pN}$. Now assume that the channel opening produces a tilt in the channel walls, changing its shape from a cylinder to a cone by an angle $\Delta\alpha$. The tilted boundary induces a bending on the membrane, which slightly changes the vertical position of the channel. For almost planar membranes, the
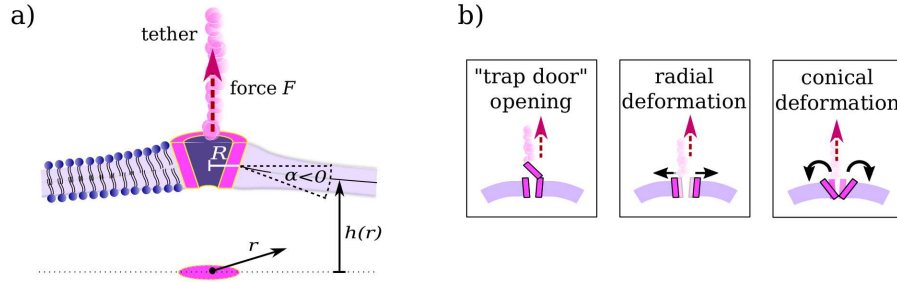
Fig. 3: *a) Sketch of a tethered membrane channel that opens when force is applied to the tether. b) Opening can proceed through a purely internal deformation (a "trap door" mechanism), but often changes the channel shape, leading to a radial or conical deformation.*

height change is $\Delta h \approx \Delta\alpha R_0 \left[\Gamma_e + \log(R_0\sqrt{\gamma/\kappa_b}/2)\right]$, where Γ_e is the Euler-Mascheroni constant and κ_b is the membrane bending modulus. A calculation of Δh is presented in Appendix A. Since a vertical force is applied to the channel, the height change Δh corresponds to a change in free energy given by

$$\Delta\mathcal{F}_{\Delta\alpha} \sim -\Delta h\, F = -\Delta\alpha F R_0 \left[\Gamma_e + \log(R_0\sqrt{\gamma/\kappa_b}/2)\right]. \tag{2}$$

The conical deformation $\Delta\alpha$ can become energetically favorable when a force F is applied to the tether. The corresponding parameter values have been measured, e.g., for the channel TREK-1 [20] and are $\Delta\alpha \sim 0.38$ rad and $R_0 \sim 2.5$ nm. With a bending modulus of $\kappa_b = 25\,k_BT$ and a typical membrane tension for eukaryotic cells of $\gamma = 10^{-3}\,k_BT/\mathrm{nm}^2 \simeq 4.1 \times 10^{-3}\,\mathrm{mN/m}$ we find $|\Delta\mathcal{F}_{\Delta\alpha}| \approx 10\,k_BT$. Thus, the gain in elastic energy through conical deformation is quite large and actually exceeds the internal energetic barrier $\sim [4-5]\,k_BT$ that resists deformation.

2.3   A topical issue: Piezo channels

A discussion of mechanosensitive membrane channels would not be complete without mentioning the molecules Piezo1 and Piezo2 [7]. During the last few years, it has become clear that Piezo proteins play critical roles in various mechanotransduction processes, including the sensing of mechanical harm (nociception), gentle touch [11], vascular functions, volume regulation of red blood cells [5], and may even play a role for the mechanical perception of oneself (proprioception) [32]. Mutations of the genes for Piezo in humans are also linked to hereditary diseases, see for example Ref. [34]. The physical mechanism underlying mechanosensing via Piezo channels in a physiological setting is a current subject of debate. They are more sensitive to mechanical stimulation than the bacterial "security valve" MscL, since the energy difference between closed and open state is only $\sim 9.7\,k_BT$ [8]. Experiments clearly demonstrate that the channels can be opened by increasing membrane tension above around $5.1\,\mathrm{mN/m}$. However, the molecules also sense cell poking and shear flow. Moreover, tethering of the membrane to the cytoskeleton or to the extracellular matrix strongly affects the response of Piezo channels. An intriguing feature of Piezo channels is that they inactivate themselves on the timescale of $100\,\mathrm{ms}$ after application of a constant force. This behavior may allow the channels to selectively respond to changes in the applied forces but reduces their sensitivity in the high-frequency regime [17].

a) mammalian cell on a substrate

actin fibers

vinculin

talin

transmembrane
adhesions
(integrins)

b) molecular structure of talin

c) stretch opens binding sites

vinculin

force   force

d)

transition
state
(TS)

unfolded
state
(1)

folded
state
(0)

free energy

"reaction coordinate"

e)

Log[k_{10}]
Log[k_{01}]

unfolding

folding

force [pN]
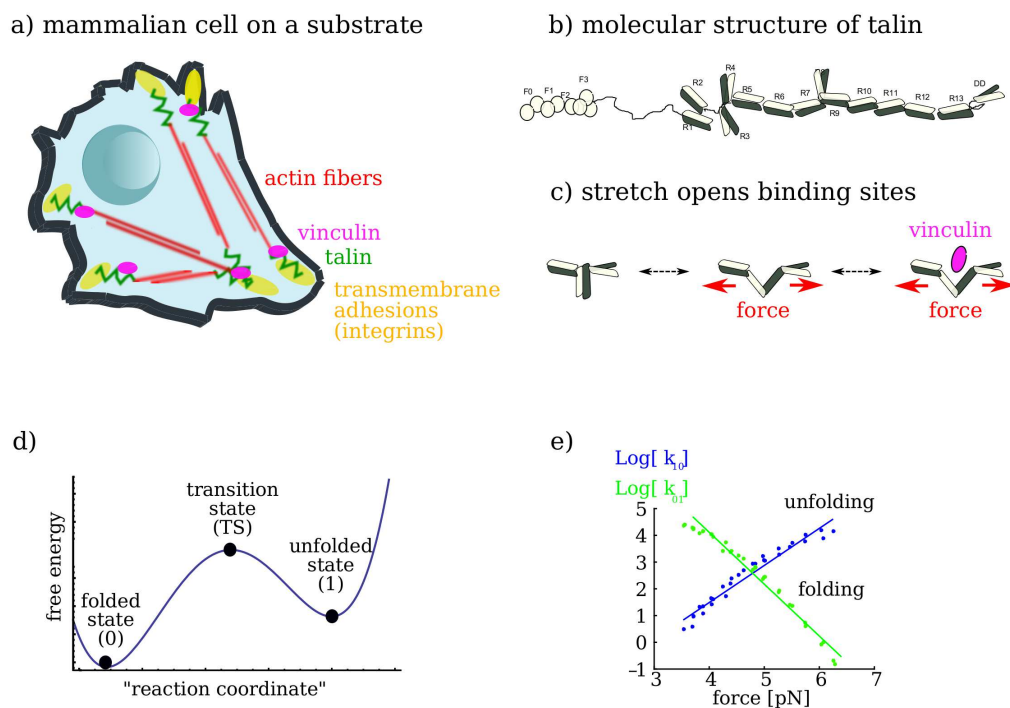
Fig. 4: *a) Many eukaryotic cells possess dedicated adhesion structures that adapt their size and composition to the mechanical load that they are exposed to. b) The molecule talin connects transmembrane integrins with the intracellular actin cytoskeleton. c) If tensile forces between $5\,\mathrm{pN}$ and $25\,\mathrm{pN}$ are applied to talin, the molecule unfolds its rod domains one after the other and thereby allows binding of an increasing number of vinculin molecules. d) sketch of a hypothetical energy landscape separating the folded and unfolded state of a single fold in absence of force. e) Measured folding and unfolding rates of the R3 domain of Talin. The straight lines are fits with Eqns. (5a, 5b). Data points were taken from Ref. [33].*

3 Stretch-sensing structural molecules

3.1 Talin responds to differential levels of stretch

Eukaryotic cells have means to detect and regulate mechanical stress in the intracellular cytoskeleton [13, 28, 6]. Key cytoskeletal proteins are filamentous actin, myosin motors that produce contractile forces in the cytoskeleton, and molecules connecting the cytoskeleton to trans-membrane integrin complexes, see Fig. 4a). One molecule that plays an essential role is talin. In recent years, evidence has emerged that talin acts as a mechanosensor, responding to applied physiological forces that are generated by the actomyosin complex to strengthen the adhesion sites connecting the cell and the extracellular matrix.

Talin comprises of a head domain and 13 rod domains that are connected by an unstructured linker chain, see Fig. 4b). The molecule is up to around $100\,\mathrm{nm}$ long when stretched and various binding sites for actin, vinculin, and integrins are distributed along its length. Some of the binding sites are cryptically buried inside the protein structure and usually not accessible to the binding partners. When integrated into the cytoskeleton, talin constitutes a force-bearing linkage between the extracellular matrix (ECM) and the actomyosin contractile machinery by binding to integrins via the F3 domain in the N-terminal head and to actin via a number of actin-

binding sites located along the talin rod [2]. In this arrangement, the domains R1 to R12 may all experience tensile forces that can lead to conformational changes making further binding sites accessible, see Fig. 4c). It has been shown that there are 11 crypic vinculin binding sites that only become exposed under increasing tensile stress [33]. Thus, the binding affinity of talin to other molecules is differentially regulated by force. Since talin has multiple binding sites that open at increasing forces, its function is somewhat reminiscent of a classical force-measurement device employing a spring and a ruler Fig. 1a).

3.2   Opening and closing of stretched molecular folds

To calculate how the unfolding of stretched molecules depends on the applied force, we consider a linear molecule with only one folded site that can unfold in a reversible manner. Folding and unfolding in the absence of forces can be pictured as a transition between two minima in the free energy landscape determined by the molecular conformation, see Fig. 4d). The process can be idealized as a diffusive motion of the system state along a one-dimensional reaction coordinate. Calculation of the transition rates across an energetic barrier is the famous Kramers problem [16]. For energy barriers that are much larger than the thermal energy scale, one finds for the transition from one minimum (state j) to the other minimum (state i) that

$$k_{ij} \approx c_0 e^{-\frac{(\mathcal{G}_{TS} - \mathcal{G}_j)}{k_B T}}, \tag{3}$$

where $\mathcal{G}_{TS}$ is the maximum of free energy at the transition state. The exponential dependence of a reaction rate on an energy divided by $k_B T$ is also known as Arrhenius law. To employ this framework for folding and unfolding of a chain-like molecule, we make the highly simplified assumption that the system behaves as an elastic spring with elastic constant d and rest length L_0 in the folded state. If the molecule unfolds, the rest length of the chain increases. The rest length is $L_0 + \delta L_1$ in the transition state and $L_0 + \delta L_1 + \delta L_2$ in the unfolded state. Hence, we can assign the following energies to the folded state (0), the transition state (TS), and the unfolded state (1)

$$\mathcal{G}_0 = \mu_0 + \frac{d}{2}(y - L_0)^2, \tag{4a}$$

$$\mathcal{G}_{TS} = \mu_{TS} + \frac{d}{2}(y - (L_0 + \delta L_1))^2, \tag{4b}$$

$$\mathcal{G}_1 = \mu_1 + \frac{d}{2}(y - (L_0 + \delta L_1 + \delta L_2))^2, \tag{4c}$$

where y represents the extension of the molecule. Employing Eq. (3) and the state-dependent force $F = d(y - L_0)$ or $F = d(y - (L_0 + \delta L_1 + \delta L_2))$ we find

$$k_{10} = c_0 e^{\frac{\mu_0 - \mu_{TS} - d\delta L_1^2/2 + \delta L_1\, d(y - L_0)}{k_B T}} = \hat{k}_{10} e^{\frac{\delta L_1}{k_B T} F}, \tag{5a}$$

$$k_{01} = c_0 e^{\frac{\mu_1 - \mu_{TS} - d\delta L_2^2/2 - \delta L_2\, d(y - (L_0 + \delta L_1 + \delta L_2))}{k_B T}} = \hat{k}_{01} e^{-\frac{\delta L_2}{k_B T} F}, \tag{5b}$$

where $\hat{k}_{10}$ and $\hat{k}_{01}$ are constants. Thus, the transition rates from one state into the other depend exponentially on the force F. The prefactors $\delta L_{1,2}/(k_B T)$ in the exponent determine how differently F affects forward and reverse rates and depend on molecular details. Note that the rates naturally satisfy a local detailed balance constraint

$$\frac{k_{01}}{k_{10}} = e^{\frac{\mathcal{G}_1 - \mathcal{G}_0}{k_B T}}, \tag{6}$$

and therefore are thermodynamically admissible. In reality, biological molecules rarely behave like ideal elastic springs and unfolding is usually a complex process involving multiple transition states and pathways. Nevertheless, Eqns. (5a, 5b) are often a good approximation, as can be seen for example by comparison with the folding rates of the R3 domain of talin, see Fig. 4e). The measured data points for this comparison were taken from Ref. [33].

4 Force measurement with a two-state sensor

4.1 A generic model for a molecular force sensor

In this section, we discuss a simple model that epitomizes the theory of molecular sensors. We idealize a force sensor, for instance a membrane channel, as a two-state system. The system state is described by the binary variable $x \in \{0, 1\}$. The rate constant for a transition $0 \to 1$ is denoted by k_{10} and the rate constant for $1 \to 0$ is denoted by k_{01}. We assume Arrhenius-type approximations for the rates

$$k_{10} = \hat{k}_{10} e^{rF}, \qquad\qquad k_{01} = \hat{k}_{01} e^{-rF}, \qquad (7)$$

where $\hat{k}_{10}$, $\hat{k}_{01}$, and r are constants. Thus, a positive force F increases the probability to be in $x = 1$ by increasing the transition rate into this state and by also decreasing the transition rate out of this state. To describe a sequence of transitions, we employ a two-state Markov process also known as random telegraph process. $P(x, t|x_0, t_0)$ is the probability to be in state x at time t given a state x_0 at time t_0. The probabilities obey

$$1 = P(1, t|x_0, t_0) + P(0, t|x_0, t_0) \qquad (8)$$

and the Master equation reads

$$\partial_t P(1, t|x_0, t_0) = -k_{01} P(1, t|x_0, t_0) + k_{10}(1 - P(1, t|x_0, t_0)). \qquad (9)$$

The steady state expectation values and variances are given by

$$\langle x \rangle_{ss} = \frac{k_{10}}{k_{10} + k_{01}}, \qquad (10)$$

$$\sigma_{ss}^2 = \langle x^2 \rangle_{ss} - \langle x \rangle_{ss}^2 = \langle x \rangle_{ss} - \langle x \rangle_{ss}^2. \qquad (11)$$

A more detailed discussion of the two-state model is presented in Appendix B.

4.2 Precision of force measurement with a two-state sensor

In this subsection, we study how the two-state sensor can be used to measure the value of the force F. The probabilities to be in either of the state are a unique function of F, as illustrated for example in Fig. 2c). Thus, cells could in principle determine the magnitude of a constant force by recording the statistics of the sensor state. If the sensor state x is monitored for a long time T, the average is $\bar{x} = \frac{1}{T} \int_0^T x \, \mathrm{d}t \approx \langle x \rangle_{ss}$. Then, an estimate for F follows from inverting $\langle x \rangle_{ss} = 1/(1 + \hat{k}_{01} e^{-2rF}/\hat{k}_{10})$, which gives

$$F \approx \log[\hat{k}_{01}\bar{x}/(\hat{k}_{10} - \hat{k}_{10}\bar{x})]/(2r). \qquad (12)$$

The error of this estimate depends on the length of the measurement time T. Since F is constant, all the error must come from the stochastic fluctuations in the sensor state, characterized by the variance of $\bar{x}$. This variance is to be calculated as $\bar{\sigma}_{ss}^2 \equiv \langle \bar{x}\bar{x} \rangle_{ss} - \langle \bar{x} \rangle_{ss}^2$. Using the correlation function (46) derived in the appendix together with Eq. (11) we find

$$\bar{\sigma}_{ss}^2 = \frac{1}{T^2} \int_0^T \int_0^T \langle x(t)x(t') \rangle_{ss} \, \mathrm{d}t\mathrm{d}t' - \langle \bar{x} \rangle_{ss}^2 \approx \frac{2}{T(k_{01} + k_{10})} \sigma_{ss}^2, \tag{13}$$

where we assumed that the measurement time is much longer than the characteristic timescale of the sensor $T \gg 1/(k_{01} + k_{10})$. The meaning of Eq. (13) is that time averaging reduces the variance in the measurement of $\bar{x}$ to leading order by a factor of $(k_{01} + k_{10})^{-1}/T$. Knowing the variance of the estimated state $\bar{x}$, we can now proceed to calculate the corresponding uncertainty in force measurement δF. A Taylor expansion for small δF yields

$$\left(\frac{\partial \bar{x}}{\partial F} \right)^2 (\delta F)^2 = \bar{\sigma}_{ss}^2. \tag{14}$$

When solving for $(\delta F)^2$ and inserting Eq. (13), we find a remarkably simple result

$$(\delta F)^2 = \frac{1}{2r^2T} \left(\frac{1}{\hat{k}_{10}e^{rF}} + \frac{1}{\hat{k}_{01}e^{-rF}} \right). \tag{15}$$

The relation implies that the uncertainty is dominated by the smaller of the two rates. Good measurements are only possible if the timescale of both state transitions is much shorter than the measurement time T. Eq. (15) is almost identical to a well-known formula for the precision of concentration sensing in biological systems, the so-called Berg-Purcell limit [4, 1, 31]. However, in the context of force sensing, Eq. (15) poses a rather stringent constraint on the range of forces that can be measured since the rates k_{ij} depend exponentially on F. The signal-to-noise ratio is $F^2/(\delta F)^2 \sim F^2 \hat{k}_{ij} T \, r^2 \exp{(-r|F|)}$. If the force-sensing module is, for example, a molecular folding site that is similar to those in talin, we expect $r \sim 5\,\mathrm{nm/k_B T} \sim 1/\mathrm{pN}$. The signal to noise ratio shows that extending the working range of such a force sensor over a range of $[0 - 10]\,\mathrm{pN}$ requires taking extensive statistics with $\hat{k}_{ij}T \gtrsim 10^3$. Note that this result only holds if both rates are force-dependent. Having one force-independent rate may be somewhat advantageous.

In summary, however, measuring the analog value of forces with a two-state sensor can be challenging. Also, one may argue that biological cells often do not need to know the precise magnitude of a mechanical stimulus. Rather, it is important to quickly detect forces, stresses, or tensions if they exceed a certain threshold. The focus of the next section will be optimal on-line detection of such events.

5   Sequential, threshold-based force sensing

One of the purposes of biological force sensing is to help conserve mechanical integrity of cells and tissue. To be able to respond to external forces appropriately, cells must be able to identify those situations where the mechanical load is too high. Typically, one can characterize destructive amounts of mechanical load by a threshold. Then, the challenge for cells is to react as quickly as possible if this threshold is surpassed. It is thus interesting to ask if there are strategies that are optimal for the detection of such events.

5.1   The CUSUM test for change detection

Consider a stochastic two-state sensor with a time-dependent state x that is affected by the signal F. The sensor could be represented, for instance, by the model introduced in Sec. 4.1. For simplicity, we assume that F changes during the observation time in a step-wise fashion from a value F_0 to a different value F_1 as shown in Fig. 5a). We will now introduce a procedure to detect this change quickly on the fly, without producing many false detections.

Denote the probability to observe a sequence of states $[x_1, \ldots, x_k]$ by $\Pi_{i=1}^k P_F(x_i)$. To quantify the relative probability of having $F = F_1$ versus $F = F_0$, we consider the logarithm of the probability ratios

$$\mathcal{L}_k = \log \left(\frac{\Pi_{i=1}^k P_{F_1}(x_i)}{\Pi_{i=1}^k P_{F_0}(x_i)} \right) = \sum_{i=1}^k \log \left(\frac{P_{F_1}(x_i)}{P_{F_0}(x_i)} \right) = \sum_{i=1}^k \Delta \mathcal{L}_i. \tag{16}$$

As long as $F \sim F_0$, the log likelihood decreases since the denominator is larger than the numerator. After the change, when $F \sim F_1$, the log likelihood increases. Hence, we can determine a change point by locating the minimum in $\mathcal{L}$ at which the function switches from a decreasing trend to an increasing trend. However, to avoid detection errors, it is advisable to wait a little bit after $\mathcal{L}$ has reached its minimum. By sampling $\mathcal{L}$ for a bit following a minimum, we ensure that we are not detecting random fluctuations but instead pick up the real trend. To constantly test if the log likelihood has a positive trend, we iteratively calculate a decision function g_k using the likelihood increments $\Delta \mathcal{L}_i = \log \left(\frac{P_{F_1}(x_i)}{P_{F_0}(x_i)} \right)$ as

$$g_k = g_{k-1} + \Delta \mathcal{L}_k \qquad \text{if } g_{k-1} + \Delta \mathcal{L}_k \geq 0, \tag{17a}$$
$$g_k = 0 \qquad \text{if } g_{k-1} + \Delta \mathcal{L}_k < 0. \tag{17b}$$

This procedure is continued until the decision function g exceeds a fixed value h. Then the decision is made that F has changed from F_0 to F_1. If we assign a time t_k to every measurement x_k, the time at which the decision is made can be formally expressed as

$$\tau_d \equiv \min(t_k | g_k > h). \tag{18}$$

A graphical illustration of the procedure is given in Fig. 5a)-c). This method for detecting changes was first suggested by E.S. Page [22] around 50 years ago. Since it is based on an evaluation of a cumulative sum, it is commonly referred to as CUSUM test. It can be shown that the CUSUM test is optimal in the following sense: if a detection threshold h is chosen such that false detections occur with a mean period that is larger than a constant γ, then the CUSUM test has the smallest worst mean delay for detection of a real change. The proof of this optimality statement is quite technical and comes in different variants, for asymptotic optimality when $\gamma \to \infty$ [19], in a Bayesian framework [26], and for continuous times and different stochastic dynamics determining $\Delta \mathcal{L}_k$ [21]. Here, we will content ourselves with an estimation of how quick the response of the CUSUM test is.

Assuming that the force change occurs at a time τ_c, the delay between τ_c and the decision time $\tau_d \geq \tau_c$ is determined by the requirement of taking a random number of m samples. To estimate m, we consider the sequence of log likelihood values just after the change occurred $\Delta \mathcal{L}_1, \Delta \mathcal{L}_2 \ldots \Delta \mathcal{L}_m$. For simplicity, we assume that the $\Delta \mathcal{L}_i$ all have the same first moment $\langle \Delta \mathcal{L}_i \rangle_{F_1} = \langle \Delta \mathcal{L} \rangle_{F_1}$ where $\langle \ldots \rangle_{F_1}$ denotes the expectation value with respect to the distribution
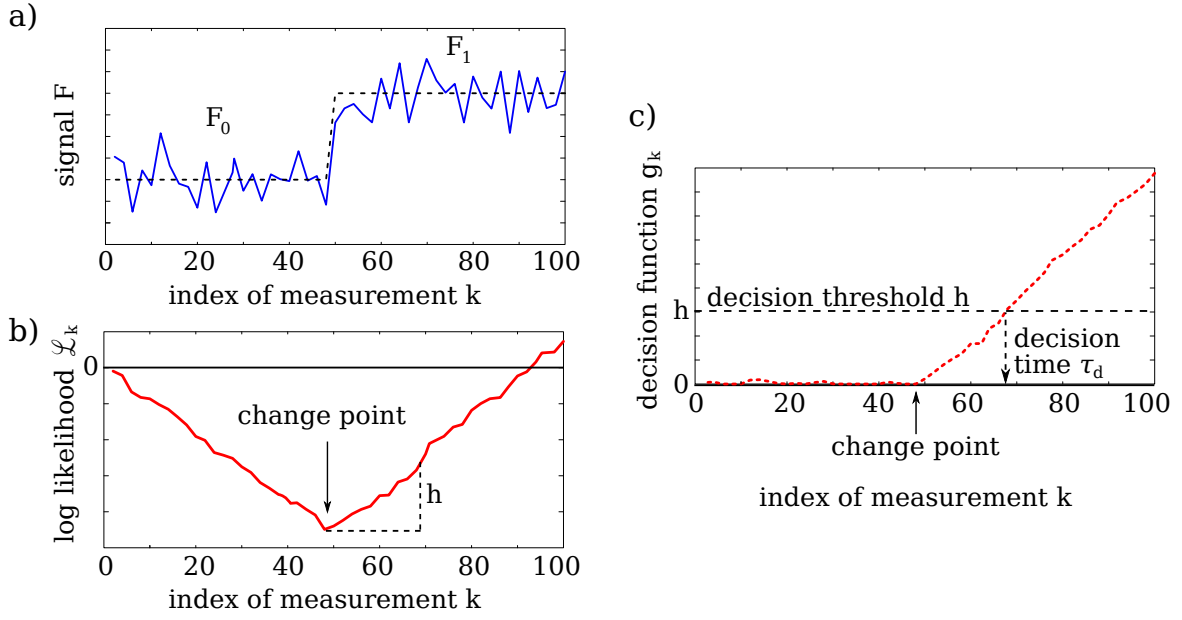
Fig. 5: *The classical CUSUM test discriminates between two values of a continuous signal. a) It is assumed that the signal F jumps between two values F_0 and F_1. Measurements are conducted at discrete times. b) The logarithmic likelihood of F_1 versus F_0 has a decreasing trend for $F \sim F_0$ and has a increasing trend for $F \sim F_1$. c) The decision function g_k records increases in the log likelihood. If $g_k \geq h$, the decision is made that F_1 is the new signal value.*

determined by F_1. We can write

$$
\begin{aligned}
\langle \sum_{i=1}^{m} \Delta \mathcal{L}_i \rangle_{F_1} &= \langle \sum_{i=1}^{\infty} \Theta(m-i) \Delta \mathcal{L}_i \rangle_{F_1} = \sum_{i=1}^{\infty} \langle \Theta(m-i) \Delta \mathcal{L}_i \rangle_{F_1} \\
&= \sum_{i=1}^{\infty} \langle \Delta \mathcal{L}_i \rangle_{F_1} \langle \Theta(m-i) \rangle_{F_1} = \langle \Delta \mathcal{L} \rangle_{F_1} \langle m \rangle_{F_1},
\end{aligned}
\tag{19}
$$

where we employed the unit step function $\Theta(y) = 0$ for $y < 0$ and $\Theta(y) = 1$ for $y \geq 0$. At the decision time τ_d, the procedure of the CUSUM test requires $\langle \sum_{i=1}^{m} \Delta \mathcal{L}_i \rangle_{F_1} \approx \langle g_k \rangle_{F_1} \approx h$. It follows from Eq. (19) that the expected number of measurements producing a delay between force change and sensor response is approximated by

$$
\langle m \rangle_{F_1} \approx \frac{h}{\langle \Delta \mathcal{L} \rangle_{F_1}} = \frac{h}{\langle \log \left(\frac{P_{F_1}(x)}{P_{F_0}(x)} \right) \rangle_{F_1}}.
\tag{20}
$$

The term in the denominator of Eq. (20) is called Kullback-Leibler divergence and is a measure for how different the two distributions P_{F_1} and P_{F_0} are. The Kullback-Leibler divergence only becomes zero if the two distributions are equal, leading to a divergent mean detection delay.

5.2   Can optimal sequential tests be realized with membrane channels?

To study a concrete example of how the CUSUM test can be important in biology, we consider a force-sensing membrane channel that is described by the two-state model introduced
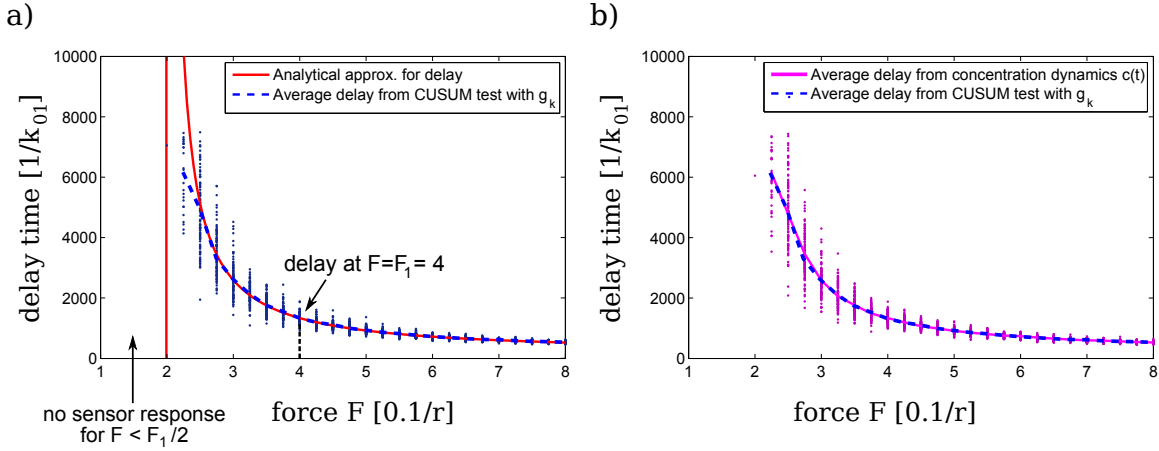
Fig. 6: *Results for detection of a sudden force change from 0 to $F > 0$ at time τ_c. The parameters of the CUSUM test are $F_0 = 0$, $F_1 = 4$, and $h = 100$. We set $r = 0.1$, $k_{01} = k_{10} = 1$. a) Simulation results for the waiting times from the proper CUSUM test, Eqns. (17a, 17b), compare well with the analytical approximation given in Eq. (26). b) The approximate CUSUM test realized with concentrations of signaling molecules $c(t)$, Eqns. (24a, 24b), responds to force changes with almost the same delay as the CUSUM test.*

in Sec. 4.1. In our two-state model, the waiting times in both states are exponentially distributed. The probability to observe a sequence of states is thus given by $P_F(\{\tau_1, \tau_2, \ldots\}) = k_{ij}e^{-k_{ij}\tau_1}dt_1\, k_{ji}e^{-k_{ji}\tau_2}d\tau_2 \ldots$ with $ij \in \{01, 10\}$, see Appendix B. The probability to observe a waiting time τ_n during which the system remains in one state $x \in \{0, 1\}$ can be conveniently written as

$$P_F(\tau_n) = e^{-(xk_{01}(F)+(1-x)k_{10}(F))\tau_n} k_{01}^{j_n^{01}}(F) k_{10}^{j_n^{10}}(F)\, d\tau. \tag{21}$$

Here, the indicator functions j_n^{01} and j_n^{10} are only non-zero if the state changes at the end of τ_n. If the system state changes as $0 \to 1$, we set $j_n^{01} = 1$ and if the change is $0 \to 1$ we set $j_n^{10} = 1$. The increment of the logarithmic likelihood is thus given by

$$\Delta\mathcal{L}(\tau_n) = \log\left(\frac{P_{F_1}(\tau_n)}{P_{F_0}(\tau_n)}\right) = (k_{01}(F_0) - k_{01}(F_1))x(t)\tau_n + j_n^{01}\log\left(\frac{k_{01}(F_1)}{k_{01}(F_0)}\right) +$$
$$(k_{10}(F_0) - k_{10}(F_1))(1 - x(t))\tau_n + j_n^{10}\log\left(\frac{k_{10}(F_1)}{k_{10}(F_0)}\right). \tag{22}$$

Next, we assume that the force is initially small and set $F_0 = 0$. Using the expressions (7) for the force-dependent transition rates yields

$$\Delta\mathcal{L}(\tau_n) = [\hat{k}_{01}(1 - e^{-rF_1}) + \hat{k}_{10}(e^{rF_1} - 1)]x(t)\tau_n - \hat{k}_{10}(e^{rF_1} - 1)\tau_n + (j_n^{01} - j_n^{10})rF_1$$
$$\sim [\hat{k}_{01}(1 - e^{-rF_1}) + \hat{k}_{10}(e^{rF_1} - 1)]x(t)\tau_n - \hat{k}_{10}(e^{rF_1} - 1)\tau_n. \tag{23}$$

In the second line we have neglected the terms $\sim \pm rF_1$ since these represent short kicks of alternating sign and therefore do not produce a continuous trend in the likelihood function.

If cells are to make use of the CUSUM test to detect a force $F_1 > 0$, the detection procedure must be implemented biochemically, which includes a repeated evaluation of Eq. (23). To see how this occurs naturally in membrane channels, we consider the dynamics of signaling molecules, e.g., calcium ions, that pass through the channel. We denote the intracellular concentration of the signaling molecule by $c(t)$ and assume that the molecule is available in excess

outside of the cell. We then have $\frac{\mathrm{d}c(t)}{\mathrm{d}t} = a\,x(t) - b(c(t))$ where a is the rate at which molecules can pass through the open channel and $b(c(t))$ denotes the rate at which the signaling molecules are removed. Typically, the molecules are being pumped actively out of the cytosol. In the case of calcium ions, an established expression for the rate of pumping is $b(c) = \hat{b}_1 c^2/(\hat{b}_2 + c^2)$ with two constants $\hat{b}_{1,2}$ [18]. Assuming that the ion pumps operate always at maximum speed, we take $\hat{b}_2 \ll c^2$ and $b(c) \approx \hat{b}_1$. Then, the concentration changes in each time step Δt as

$$c(t + \Delta t) \approx c(t) + ax(t)\Delta t - \hat{b}_1 \Delta t \qquad \text{if } c(t) + ax(t)\Delta t - \hat{b}_1 \Delta t \geq 0, \qquad (24a)$$

$$c(t + \Delta t) = 0 \qquad \text{if } c(t) + ax(t)\Delta t - \hat{b}_1 \Delta t < 0. \qquad (24b)$$

The concentration increment in Eq. (24a) has the same form as the likelihood increment given in Eq. (23), except that the waiting times τ_n are replaced by infinitesimal time steps Δt. The concentration $c(t)$ also obeys the same dynamics as the decision function g_k for the CUSUM test, Eqns. (17a,17b). Therefore, we suggest that $c(t)$ can act as a continuous approximation for g_k to decide whether the force has exceeded a prescribed threshold. The reaction parameters a and $\hat{b}_1$ determine the force $F_1 > 0$ and comparison with Eq. (23) yields

$$a/\hat{b}_1 = [\hat{k}_{01}(1 - e^{-rF_1}) + \hat{k}_{10}(e^{rF_1} - 1)]/[\hat{k}_{10}(e^{rF_1} - 1)]. \qquad (25)$$

The threshold in $c(t)$ leading to a detection of a force can be realized, for example, by a chemical reaction that depends non-linearly on $c(t)$ to produce a step-like response if $c(t) \geq \tilde{h}$.

To estimate the delay until detection we consider the waiting time probability of consecutive closed and open states $P_F(\tau_0, \tau_1) = k_{10}(F)e^{-k_{10}(F)\tau_0}\,\mathrm{d}\tau_0\ k_{01}(F)e^{-k_{01}(F)\tau_1}\,\mathrm{d}\tau_1$. Using the same reasoning as for Eq. (20), we obtain the average number of consecutive pairs of state changes at force F as

$$\langle m_{\mathrm{oc}} \rangle_F \approx \frac{h}{\int \int_0^\infty \log\left(\frac{P_{F_1}(\tau_0, \tau_1)}{P_{F_0}(\tau_0, \tau_1)}\right) P_F(\tau_0, \tau_1)\,\mathrm{d}\tau_0 \mathrm{d}\tau_1} = \frac{h}{2[\cosh(rF) - \cosh(rF_1 - rF)]}. \qquad (26)$$

With the average number of state-change pairs given, an approximate delay time results as $\langle(\tau_0 + \tau_1)\rangle_F \langle m_{\mathrm{oc}} \rangle_F = (1/k_{10}(F) + 1/k_{01}(F))\,\langle m_{\mathrm{oc}} \rangle_F$.

In Fig. 6a), results from a simulation of the CUSUM test for detection of a suddenly applied force F are presented. The likelihood is calculated with the constant parameter $F_1 = 4 \times 0.1/r$, while the true magnitude of the force F is varied. It can be seen the sensor only responds for $F > F_1/2$. Moreover, the sensor responds to forces that are above the threshold $F > F_1$ on average faster than for $F = F_1$. The analytical approximation for the delay time agrees well with the simulation results. Figure 6b) shows a comparison of the proper CUSUM test based on evaluation of g_k, Eqns. (17a, 17b), with the approximate biological realization based on the concentration of signaling molecules $c(t)$, Eqns. (24a, 24b). Clearly, the performance of the biological realization is very similar to the performance of the full CUSUM test. Therefore, we can surmise that biology employs a signal integration strategy like the CUSUM test if optimal detection of forces is required.

Finally, we mention that membrane-channel systems combined with a threshold-like response to a critical concentration of signaling molecules is a common motive in cell biology. Examples include depolarization of nerve cells and local intracellular calcium responses. It is tempting to conclude that signal integration principles akin to those idealized by the CUSUM test are a generic feature of such systems.

Appendices

A Mechanical interaction of a channel with the surrounding membrane

A.1 Calculation of the membrane deformation

We assume that the membrane-channel system is in mechanical equilibrium and consider an almost planar lipid membrane. The height h of the membrane above a reference plane is to be a unique function of a two-dimensional position vector $\mathbf{r}$ lying in the reference plane. For the position vector, we employ a cylindrical coordinate system with radius r and angular coordinate φ, see Fig. 3. The nabla operator ∇ operates in the two-dimensional reference plane and, since we assume small gradients, the functional determinant is approximated as $\sqrt{1 + (\nabla h)^2} \approx [1 + \frac{1}{2}(\nabla h)^2]$. Within this framework, a fluid membrane can be described with the following energy

$$\mathcal{H}_h = \int \frac{\kappa_{\mathrm{b}}}{2}(\nabla^2 h)^2 + \gamma[1 + \frac{1}{2}(\nabla h)^2]\mathrm{d}^2 r, \tag{27}$$

where the surface integration extends over the entire membrane. Here, κ_{b} is the bending constant of the membrane and γ is the membrane tension. The first term in Eq. (27) is an energy penalty resulting from non-zero mean curvature while the second term penalizes changes of the area. A variation of the energy yields

$$\delta\mathcal{H}_h = \int \kappa_{\mathrm{b}}(\nabla^2 h)(\delta\nabla^2 h) + \gamma(\nabla h)(\delta\nabla h)\mathrm{d}^2 r = \int \nabla^2(\kappa_{\mathrm{b}}\nabla^2 h - \gamma h)\delta h\, \mathrm{d}^2 r$$
$$+ \int [\kappa_{\mathrm{b}}\nabla^2 h(\delta\nabla h) - \nabla(\kappa_{\mathrm{b}}\nabla^2 h - \gamma h)(\delta h)]\, \mathbf{s}\mathrm{d}s, \tag{28}$$

where we employed partial integration and the divergence theorem with $\mathbf{s}$ denoting a normal vector pointing outwards from the membrane area on the contour path s. Since $\mathcal{H}_h$ is minimal in mechanical equilibrium, the equation determining h follows from the first line of Eq. (28) as

$$\nabla^2(\nabla^2 - \xi^2)h = 0, \tag{29}$$

with $\xi^2 \equiv \gamma/\kappa_{\mathrm{b}}$. We next assume that the membrane forms a radially symmetric annulus around a circular channel protein with radius R. The membrane extends far out to a radius $L \gg R$. At the outer contour of the membrane, we fix the membrane height and slope as

$$h(L) = 0, \tag{30a}$$
$$\partial_r h(r)|_{r=L} = 0. \tag{30b}$$

For the inner contour surrounding the channel we assume the boundary conditions sketched in Fig. 3a) with a height $h(R)$ and a contact angle α given by

$$h(R) = h(0), \tag{31a}$$
$$\partial_r h(r)|_{r=R} = \alpha. \tag{31b}$$

If a constant vertical force F is applied via the tether at $r = 0$, we need to employ a free energy that takes the constant force acting on the membrane contour into account

$$\mathcal{F} = \mathcal{H}_h - \int_0^{2\pi} \frac{Fh(R)}{2\pi R} R \mathrm{d}\varphi. \tag{32}$$

The variation $\delta\mathcal{F}$ yields the expression (28) minus $1/(2\pi) \int_0^{2\pi} F \delta h(R) \, \mathrm{d}\varphi$. When calculating $\delta\mathcal{F}$, the first term in the second line of Eq. (28) is irrelevant since the contact angle at the channel is fixed by Eq. (31b). A vanishing $\delta\mathcal{F}$ in mechanical equilibrium requires

$$F = -\kappa 2\pi \partial_r \left(\xi^2 h - \nabla^2 h \right) r|_{r=R}, \tag{33}$$

as well as equation (29) for the interior of the membrane. These equations determine h completely. The solution fulfilling the above differential equations and boundary conditions is

$$h = \frac{F \log(L/r)}{2\gamma\pi} - \frac{(F + 2R\alpha\gamma\pi)K_0(r\xi)}{2R\gamma\pi\xi K_1(R\xi)}, \tag{34}$$

where K_n are the Bessel K functions of n-th order and we have dropped all terms that decay exponentially with $\xi L \ll 1$. Usually, the membrane tension is weak enough to guarantee that the lengthscale ξ^{-1} set by the tension and bending constant is much larger than the nanometer-scale that is characteristic for membrane channels. Hence, we assume $\xi r \ll 1$ and $\xi R \ll 1$ to obtain

$$h \approx \frac{F}{2\gamma\pi} \log(L/r) + \frac{(F + 2\alpha\gamma\pi R)}{2\gamma\pi} \left[\Gamma_e + \log\left(R\xi/2 \right) \right], \tag{35}$$

where Γ_e is the Euler-Mascheroni constant. If F is held constant and α changes, the resulting height change is $\Delta h = \Delta\alpha R \left[\Gamma_e + \log(R\xi/2) \right]$, which is the expression used in the main text.

A.2   Free energy of the membrane around a tethered channel

For a full analysis of how the force F changes the free energy of the membrane-channel system, we need to calculate the expression in (32) explicitly. On employing the the identity $(\nabla h)^2 = \nabla \cdot (h\nabla h) - h\nabla^2 h$ along with Eq. (29), the deformation energy becomes

$$\mathcal{H}_h = -\frac{\gamma}{2} \int h \partial_r h \, r \mathrm{d}\varphi_b|_{r=R} + \frac{\gamma}{2} \int h \partial_r h \, r \mathrm{d}\varphi_b|_{r=L} - \frac{\gamma}{2} \int h^H \nabla^2 h^S \mathrm{d}^2 r, \tag{36}$$

where h^H and h^S are the parts of h that fulfill $\nabla^2 h^H = 0$ and $(\nabla^2 + \xi^2)h^S = 0$. Again, we ignore terms that decay exponentially with $\xi L \gg 1$ and obtain up to an L-dependent constant

$$\mathcal{H}_h = -\gamma\pi R^2 - \frac{F^2 K_0(R\xi)}{4R\gamma\pi\xi K_1(R\xi)} + \frac{F^2 \log(L/R)}{4\gamma\pi} + \frac{(2R\gamma\pi\alpha)^2 K_0(R\xi)}{4R\gamma\pi\xi K_1(R\xi)}. \tag{37}$$

The work related to application of force F is given by

$$Fh(0) = Fh(R) = \frac{F^2 \log(L/R)}{2\gamma\pi} - \frac{(F^2 + 2R\gamma\pi\alpha F)K_0(R\xi)}{2R\gamma\pi\xi K_1(R\xi)}. \tag{38}$$

Adding the last two equations, we obtain for the overall free energy

$$\mathcal{F} = -\gamma\pi R^2 + \frac{(F + 2\pi\kappa_b\xi^2 R\alpha)^2}{4\pi\kappa_b\xi^2} \frac{K_0(R\xi)}{R\xi K_1(R\xi)} - \frac{F^2 \log(L/R)}{4\pi\gamma}. \tag{39}$$

We can again expand this result for $\xi R \ll 1$ to obtain

$$\mathcal{F} \approx -\gamma\pi R^2 - \alpha R F \left[\Gamma_e + \log\left(R\xi/2 \right) \right] - \frac{F^2}{4\pi\gamma} \left[\Gamma_e + \log\left(L\xi/2 \right) \right]. \tag{40}$$

B   Review of the stochastic two-state process

We consider a binary state variable $x \in \{0, 1\}$ and denote by $P(x, t | x_0, t_0)$ the probability to be in state x at time t given a state x_0 at time t_0. The probabilities obey

$$1 = P(1, t | x_0, t_0) + P(0, t | x_0, t_0) \tag{41}$$

and the probabilities evolve according to

$$\partial_t P(1, t | x_0, t_0) = -k_{01} P(1, t | x_0, t_0) + k_{10}(1 - P(1, t | x_0, t_0)). \tag{42}$$

The solution is for $P(x, t | x_0, t_0)$ is

$$P(x, t | x_0, t_0) = \frac{k_{10} \delta_{x,1} + k_{01} \delta_{x,0}}{k_{10} + k_{01}} + (\delta_{x,1} - \delta_{x,0}) \frac{e^{-(k_{10} + k_{01})(t - t_0)}}{k_{10} + k_{01}} (k_{01} \delta_{x_0,1} - k_{10} \delta_{x_0,0}), \tag{43}$$

The steady-state expectation values are thus given by

$$\langle x \rangle_{ss} = \lim_{t \to \infty} \sum_{x=1,0} x P(x, t | x_0, 0) = \frac{k_{10}}{k_{10} + k_{01}}, \tag{44}$$

$$\sigma_x^2 = \langle x^2 \rangle_{ss} - \langle x \rangle_{ss}^2 = \langle x \rangle_{ss} - \langle x \rangle_{ss}^2. \tag{45}$$

The two-time correlations for $t \geq t'$ in steady state are given by

$$\langle x(t) x(t') \rangle_{ss} = \lim_{t'' \to -\infty} \sum_{x,x',x''=1,0} x P(x, t | x', t') x' P(x', t' | x'', t'') = P(1, t | 1, t') \langle x \rangle_{ss}$$

$$= \frac{k_{10}^2 + k_{10} k_{01} e^{-(k_{10} + k_{01})(t - t')}}{(k_{10} + k_{01})^2} = \langle x \rangle_{ss}^2 + \frac{k_{10} k_{01} e^{-(k_{10} + k_{01})(t - t')}}{(k_{10} + k_{01})^2}. \tag{46}$$

Next, we aim to calculate the likelihood of a given sequence of states and start by considering a single state change. Assuming that the state is initially given by $j \in \{0, 1\}$ with $x = j$ at $t = t_0$, we are looking for the survival probability $G(\tau | j, t_0)$ that quantifies how likely it is that the system remains in the same state for a time τ. The evolution equation for the two-state process dictates that $G(\tau | j, t_0)$ obeys

$$\partial_\tau G(\tau | j, t_0) = -k_{ij} G(\tau | j, t_0). \tag{47}$$

Note that this equation also holds if the rates are time-dependent. Assuming constant rates, the differential equation yields $G(\tau | j, t_0) = e^{-k_{ij} \tau}$. We are now interested in the probability $p(\tau | j, t_0) \, d\tau$ that the state survives until τ and then changes in the infinitesimal time interval $[t + \tau, t + \tau + d\tau)$. Using the expression Eq. (47) for the rate of occurrence of the change, we have

$$p(\tau | j, t_0) \, d\tau = -\partial_\tau G(\tau | j, t_0) \, d\tau = k_{ij} e^{-k_{ij} \tau} \, d\tau. \tag{48}$$

Next, let us consider a given sequence of changes with waiting times $\{\tau_1, \tau_2, \tau_3 \ldots\}$ starting at $x = j$. Using the probability density $p(\tau | j, t_0)$ derived above, the probability of finding this given sequence is

$$P(\{\tau_1, \tau_2, \tau_3 \ldots\}) = k_{ij} e^{-k_{ij} \tau_1} d\tau_1 \, k_{ji} e^{-k_{ji} \tau_2} d\tau_2 \, k_{ij} e^{-k_{ij} \tau_3} d\tau_3 \ldots \tag{49}$$

References

[1] G. Aquino, N. S. Wingreen, and R. G. Endres. Know the single-receptor sensing limit? think again. *J. Stat. Phys.*, 162(5):1353, 2016.

[2] K. Austen, P. Ringer, A. Mehlich, A. Chrostek-Grashoff, C. Kluger, C. Klingner, B. Sabass, R. Zent, M. Rief, and C. Grashoff. Extracellular rigidity sensing by talin isoform-specific mechanical linkages. *Nat. Cell Biol.*, 17(12):1597, 2015.

[3] N. Bavi, Y. A. Nikolaev, O. Bavi, P. Ridone, A. D. Martinac, Y. Nakayama, C. D. Cox, and B. Martinac. Principles of mechanosensing at the membrane interface. In *The Biophysics of Cell Membranes*, page 85. Springer, 2017.

[4] H. C. Berg and E. M. Purcell. Physics of chemoreception. *Biophys. J.*, 20(2):193, 1977.

[5] S. M. Cahalan, V. Lukacs, S. S. Ranade, S. Chien, M. Bandell, and A. Patapoutian. Piezo1 links mechanical forces to red blood cell volume. *Elife*, 4:e07370, 2015.

[6] B. Chen, B. Ji, and H. Gao. Modeling active mechanosensing in cell–matrix interactions. *Annu. Rev. Biophys.*, 44:1, 2015.

[7] B. Coste, J. Mathur, M. Schmidt, T. J. Earley, S. Ranade, M. J. Petrus, A. E. Dubin, and A. Patapoutian. Piezo1 and piezo2 are essential components of distinct mechanically activated cation channels. *Science*, 330(6000):55, 2010.

[8] C. D. Cox, C. Bae, L. Ziegler, S. Hartley, V. Nikolova-Krstevski, P. R. Rohde, C.-A. Ng, F. Sachs, P. A. Gottlieb, and B. Martinac. Removal of the mechanoprotective influence of the cytoskeleton reveals piezo1 is gated by bilayer tension. *Nat. Commun.*, 7(10366), 2016.

[9] N. Dan and S. A. Safran. Effect of lipid characteristics on the structure of transmembrane proteins. *Biophys. J.*, 75(3):1410, 1998.

[10] T. Effertz, B. Nadrowski, D. Piepenbrock, J. T. Albert, and M. C. Göpfert. Direct gating and mechanical integrity of drosophila auditory transducers require trpn1. *Nat. Neurosci.*, 15(9):1198, 2012.

[11] A. Faucherre, J. Nargeot, M. E. Mangoni, and C. Jopling. piezo2b regulates vertebrate light touch response. *J. Neurosci.*, 33(43):17089, 2013.

[12] S. L. Geffeney, J. G. Cueva, D. A. Glauser, J. C. Doll, T. H.-C. Lee, M. Montoya, S. Karania, A. M. Garakani, B. L. Pruitt, and M. B. Goodman. Deg/enac but not trp channels are the major mechanoelectrical transduction channels in a c. elegans nociceptor. *Neuron*, 71(5):845, 2011.

[13] B. Geiger, J. P. Spatz, and A. D. Bershadsky. Environmental sensing through focal adhesions. *Nat. Rev. Mol. Cell Biol.*, 10(1):21, 2009.

[14] F. Guharay and F. Sachs. Stretch-activated single ion channel currents in tissue-cultured embryonic chick skeletal muscle. *J. Physiol.*, 352(1):685, 1984.

[15] J. Howard and S. Bechstedt. Hypothesis: a helix of ankyrin repeats of the nompc-trp ion channel is the gating spring of mechanoreceptors. *Curr. Biol.*, 14(6):R224, 2004.

[16] H. A. Kramers. Brownian motion in a field of force and the diffusion model of chemical reactions. *Physica*, 7(4):284, 1940.

[17] A. H. Lewis, A. F. Cui, M. F. McDonald, and J. Grandl. Transduction of repetitive mechanical stimuli by piezo1 and piezo2 ion channels. *Cell Rept.*, 19(12):2572, 2017.

[18] Y.-X. Li and J. Rinzel. Equations for insp3 receptor-mediated [ca2+] oscillations derived from a detailed kinetic model: a hodgkin-huxley like formalism. *J. Theo. Biol.*, 166(4):461, 1994.

[19] G. Lorden. Procedures for reacting to a change in distribution. *Ann. Math. Stat.*, 42(6):1897, 1971.

[20] G. Maksaev, A. Milac, A. Anishkin, H. R. Guy, and S. Sukharev. Analyses of gating thermodynamics and effects of deletions in the mechanosensitive channel trek-1: comparisons with structural models. *Channels*, 5(1):34, 2011.

[21] G. V. Moustakides. Optimality of the cusum procedure in continuous time. *Ann. Stat.*, 32(1):302, 2004.

[22] E. S. Page. Continuous inspection schemes. *Biometrika*, 41(1-2):100, 1954.

[23] R. Phillips, T. Ursell, P. Wiggins, and P. Sens. Emerging roles for lipids in shaping membrane-protein function. *Nature*, 459(7245):379, 2009.

[24] M. Prager-Khoutorsky, A. Khoutorsky, and C. W. Bourque. Unique interweaved microtubule scaffold mediates osmosensory transduction via physical interaction with trpv1. *Neuron*, 83(4):866, 2014.

[25] S. S. Ranade, R. Syeda, and A. Patapoutian. Mechanically activated ion channels. *Neuron*, 87(6):1162, 2015.

[26] Y. Ritov. Decision theoretic optimality of the cusum procedure. *Ann. Stat.*, 18(3):1464, 1990.

[27] B. Sabass and H. A. Stone. Role of the membrane for mechanosensing by tethered channels. *Phys. Rev. Lett.*, 116(25):258101, 2016.

[28] U. S. Schwarz and S. A. Safran. Physics of adherent cells. *Rev. Mod. Phys.*, 85(3):1327, 2013.

[29] S. Sukharev and D. P. Corey. Mechanosensitive channels: multiplicity of families and gating paradigms. *Sci. STKE*, 2004(219):re4, 2004.

[30] S. I. Sukharev, W. J. Sigurdson, C. Kung, and F. Sachs. Energetic and spatial parameters for gating of the bacterial large conductance mechanosensitive channel, mscl. *J. Gen. Physiol.*, 113(4):525, 1999.

[31] P. R. ten Wolde, N. B. Becker, T. E. Ouldridge, and A. Mugler. Fundamental limits to cellular sensing. *J. Stat. Phys.*, 162(5):1395, 2016.

[32] S.-H. Woo, V. Lukacs, J. C. De Nooij, D. Zaytseva, C. R. Criddle, A. Francisco, T. M. Jessell, K. A. Wilkinson, and A. Patapoutian. Piezo2 is the principal mechanotransduction channel for proprioception. *Nat. Neurosci.*, 18(12):1756, 2015.

[33] M. Yao, B. T. Goult, B. Klapholz, X. Hu, C. P. Toseland, Y. Guo, P. Cong, M. P. Sheetz, and J. Yan. The mechanical response of talin. *Nat. Commun.*, 7(11966), 2016.

[34] R. Zarychanski, V. P. Schulz, B. L. Houston, Y. Maksimova, D. S. Houston, B. Smith, J. Rinehart, and P. G. Gallagher. Mutations in the mechanotransduction protein piezo1 are associated with hereditary xerocytosis. *Blood*, 120(9):1908, 2012.

[35] W. Zhang, L. E. Cheng, M. Kittelmann, J. Li, M. Petkovic, T. Cheng, P. Jin, Z. Guo, M. C. Göpfert, L. Y. Jan, et al. Ankyrin repeats convey force to gate the nompc mechanotransduction channel. *Cell*, 162(6):1391, 2015.